photonics

MDPI

Article

Carbon Monoxide Detection Based on the Carbon Nanotube-Coated Fiber Gas Sensor

Yin Zhang [1,*], Wenwen Yu [1], Dibo Wang [2,3], Ran Zhuo [2,3], Mingli Fu [2,3] and Xiaoxing Zhang [1,4]

[1] Hubei Engineering Research Center for Safety Monitoring of New Energy and Power Grid Equipment, Hubei University of Technology, Wuhan 430068, China
[2] CSG Electric Power Research Institute Co., Ltd., Guangzhou 510080, China
[3] United Laboratory of Advanced Electrical Materials and Equipment Support Technology, CSG, Guangzhou 510080, China
[4] Xiangyang Industrial Institute of Hubei University of Technology, Xiangyang 441100, China
* Correspondence: yinz@hbut.edu.cn

Abstract: Accurate detection of the internal decomposition components of SF_6 electrical equipment plays an important role in the evaluation of equipment status. However, gas samples are usually taken out for detection at present, which makes it difficult to understand the real situation inside the equipment. In this paper, a carbon nanotube-coated fiber gas sensor is proposed, which has the potential to be applied as a built-in gas sensor. The fiber loop ring-down (FLRD) gas detection system based on the carbon nanotube-coated fiber gas sensor was built, and the detectable decomposition components among the four typical SF_6 decomposition components of SO_2, SO_2F_2 and SOF_2 and CO were analyzed. The results showed that the fiber gas sensor was most sensitive to CO. Based on density functional theory, it was found that single-walled carbon nanotubes had the best adsorption effect on CO molecules under the same conditions, with the adsorption energy reaching −0.150 Ha. The detection performance of the system for CO was studied, and the results showed that there was a good linear relationship between CO concentration and ring-down time: R^2 was 0.984, the maximum inversion error of 0~200 ppm CO was 1.916 ppm, and the relative error was 4.10%. The sensitivity of the system was 0.183 ns/ppm, and the detection limit of the system was 19.951 ppm. The system had good stability, with the standard deviation of single-point repeatability being 0.00356, and the standard deviation of the long period of the experiment being 0.00606. The research results provide a new idea for the detection of SF_6 decomposition components, and lay the foundation for the component detection method of built-in fiber sensor of SF_6 electrical equipment.

Keywords: SF_6 electrical equipment; carbon nanotube-coated fiber; gas sensor; CO detection; FLRD

Citation: Zhang, Y.; Yu, W.; Wang, D.; Zhuo, R.; Fu, M.; Zhang, X. Carbon Monoxide Detection Based on the Carbon Nanotube-Coated Fiber Gas Sensor. *Photonics* **2022**, *9*, 1001. https://doi.org/10.3390/photonics9121001

Received: 30 November 2022
Accepted: 16 December 2022
Published: 19 December 2022

1. Introduction

The safe and reliable operation of electrical equipment is the first defense line to avoid major accidents in the power system. Accurately grasping the operation status of electrical equipment and diagnosing its internal defect types is one of the keys to ensure the safe production of power grids and achieve efficient equipment maintenance [1,2]. SF_6 gas is widely used in gas-insulated electrical equipment due to its good arc extinguishing properties and insulating properties. However, according to existing research, SF_6 electrical equipment inevitably introduces defects in the process of manufacturing, transportation and maintenance. If the defects cannot be found in time, they gradually develop and cause equipment failure [3,4]. In the early stage of the defect, partial discharge inside the equipment is caused, which leads to the decomposition of SF_6 to produce gas decomposition components, such as CO, SO_2, SO_2F_2, SOF_2, etc. [5,6]. Monitoring these characteristic components can provide a basis for judging the type, and severity, of a defect [7,8]. Therefore, accurate monitoring of SF_6 characteristic decomposition components is of great significance

for diagnosing early latent faults of gas-insulated equipment and ensuring the safe and reliable operation of power grids.

At present, the on-site detection of SF_6 characteristic decomposition components mainly adopts electrochemical sensors and spectral detection instruments [9–13]. Zhang et al. proposed using a TiO_2 nanotube array sensor to detect SF_6 decomposition components, and realized SO_2 detection of 10–50 ppm [9]. Gui et al. used a Ni-modified carbon nanotube gas sensor to carry out theoretical and experimental studies on the detection of SF_6 decomposition components H_2S, SOF_2, SO_2 and SO_2F_2, and the detection limit reached 1 ppm [10]. Li et al. proposed a gas detection method based on $TiO_2/NiSO_4$ composite nanofibers, which could maximize the sensing response of 100 ppm SO_2F_2 by up to 189% at room temperature [11]. Zhang et al. used mid-infrared laser spectroscopy to detect SO_2F_2 and SOF_2, and the detection limit could reach 1 ppm [12]. Chen et al. studied CO detection using a 2.33 um laser and cantilever photoacoustic spectroscopy, and the detection limit reached 5.1 ppm [13]. In general, electrochemical sensors are low cost and have high detection sensitivity, but may be affected by strong electromagnetic interference in the field. The spectral detection instruments have high sensitivity, strong anti-electromagnetic interference ability and fast response speed. However, this method is based on gas absorption spectroscopy and the Lambert–Beer law. Since the background gas inside the electrical equipment is SF_6, which has strong absorption in the infrared band, it affects the detection results [14]. In addition, the above two methods both need to collect samples through the inlet port of the equipment for measurement when the methods are applied in the field. On the one hand, this consumes SF_6 gas inside the equipment. On the other hand, it may only detect the gas component in the area near the inlet port of the equipment. It is difficult to grasp the real component content inside the equipment, and it is impossible to truly realize the online monitoring of the SF_6 decomposition components inside the equipment.

Optical fiber sensors have the advantages of strong anti-electromagnetic interference ability, good insulation performance, high sensitivity and low cost, and are widely used in the field of sensing. Optical fiber sensors generally reflect changes in the physical parameters (temperature, stress, ultrasound, etc.) to be measured, by measuring changes in signals, such as light intensity, refractive index, and wavelength [15,16]. The adsorption of a specific gas by a nanomaterial causes a change in its dielectric constant (this is also the principle of an electrochemical sensor) [17]. If the nanomaterial is used as an optical fiber layer, when the nanomaterial adsorbs gas, it indirectly causes its refractive index to change, which causes light changes and achieves gas detection [18]. The nanomaterial-coated optical fiber gas sensor has the advantages of strong electromagnetic interference resistance, simple structure and good insulation performance [19,20], and it is very suitable as a built-in detection method for the characteristic gas components of the SF_6 electrical equipment. At present, there are few studies on gas sensors of nanomaterial-coated optical fiber. Some scholars have explored its gas sensing characteristics [21,22], and realized gas detection at the ppm level. However, its detection performance still has some gaps with existing nanomaterial-based gas sensors and spectral detection methods. It is necessary to further improve the demodulation method and the optical path structure.

In this paper, a preliminary study on a nanomaterial-coated optical fiber gas sensor for the detection of SF_6 decomposition components was carried out, and a carbon nanotube thin film optical fiber gas sensor prepared. Based on the fiber loop ring-down (FLRD) system, the gas sensing properties of the gas sensor for SF_6 gas components were explored, and the detection of SF_6 decomposition components, based on the carbon nanotube-fiber sensor, realized. The research results provide new ideas for future research on the online monitoring technology of SF_6 electrical equipment.

2. Method

2.1. Preparation Method of Coated Optical Fiber

In the experiment, a carbon nanotube fiber sensor was prepared by using a single-mode fiber. The cladding and coating of the single-mode fiber were stripped off to obtain

the bare fiber, which was preheated with a butane flame. At the same time, both ends of the fiber were pulled to make the coating area steady, and continuously heated for 4 s. Then, the tapered optical fiber was moved to a clean glass slide to fix it, and a water dispersion solution of 0.15 wt% carboxylated high-purity single-walled carbon nanotubes was applied to the glass slide substrate. The optical fiber was baked in a constant temperature oven at 75 °C for 40 min, and, finally, the coated optical fiber was taken out and put into a closed air chamber as a fiber gas sensor. The gas detection cell is shown in Figure 1.

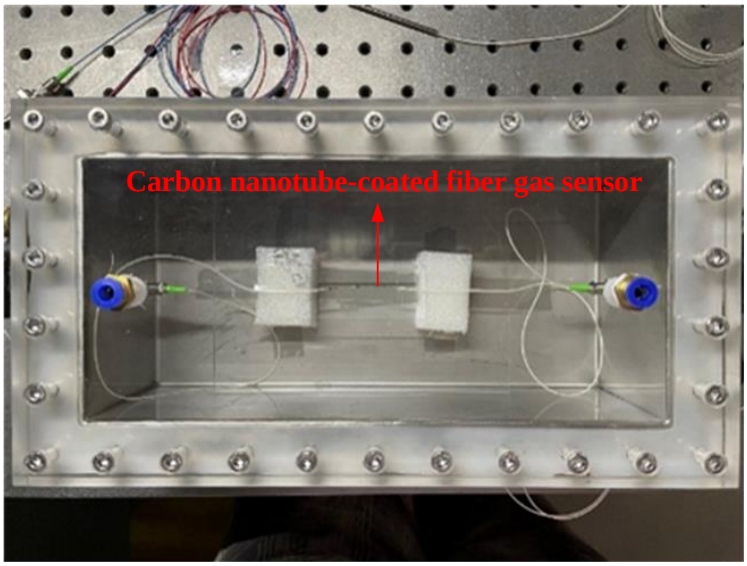

Figure 1. Gas detection cell.

2.2. FLRD Gas Detection System

The FLRD system was used for the gas detection experiment. The FLRD system realized signal demodulation by establishing the relationship between the ring-down time and the optical loss of the fiber sensor, which was not easily affected by the fluctuation of the light source, and was suitable for various types of optical fiber sensors. The FLRD system built in this paper is shown in Figure 2. The system consisted of a function signal generator, a laser source, an isolator, two 1 × 2 fiber couplers, a gas detection cell with the carbon nanotube-coated fiber gas sensor, a photodetector (PD), an oscilloscope, etc.

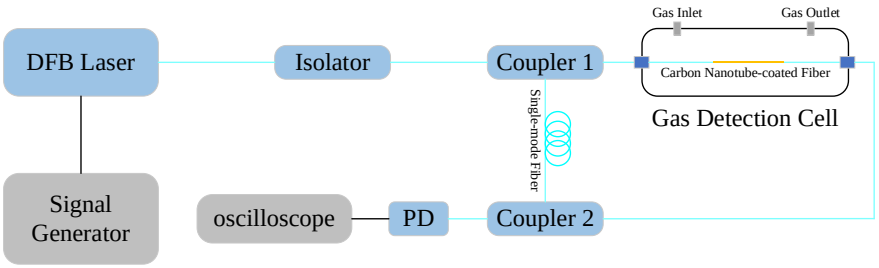

Figure 2. The FLRD system for gas detection.

The DFB laser (having a center wavelength of 1530 nm, and a linewidth of 2 MHz) was modulated by the function signal generator. The single-mode fiber ring length was 1014 m. The modulated laser signal passed through the isolator to make it transmit in one direction so as to avoid damage to the laser by reverse light. The incident laser entered the ring cavity through Coupler 1, passed through the carbon nanotube-coated fiber gas sensor, and then entered Coupler 2. The laser energy was split into two parts in Coupler 2. Most of the laser energy passed through the ring cavity and then entered Coupler 1 and circulated in the ring cavity. Another part of the laser energy was output to the PD, and, finally, the

ring-down waveform was output on the oscilloscope. The laser interacted with the sensor once per cycle, so the sensitivity increased as the number of cycles increased. Considering the different system losses caused by couplers with different split ratios, this would affect the number of cycles of the laser in the ring cavity. Therefore, the appropriate split ratio of the couplers was determined by experiment to improve the detection sensitivity.

3. Results

3.1. The Coupler Split Ratio Determination

The detection result obtained by the FLRD system was a series of attenuated pulse waveforms, and the selection of the coupler split ratio would affect the optical loss of the system, which would affect the number of pulses, and the number of pulses relates to the accuracy of curve fitting. Therefore, it was necessary to determine the optimal coupler split ratio of the FLRD system.

The FLRD system was set to a frequency of 8 kHz and a duty cycle of 2%. The Gas detection cell was filled with N_2 as the background gas, and the detection results of the couplers with different split ratios were analyzed under the background gas. The split ratio adopted three common couplers of 1:99, 10:90, and 50:50, and the results under different collocations were obtained, as shown in Figure 3 and Table 1.

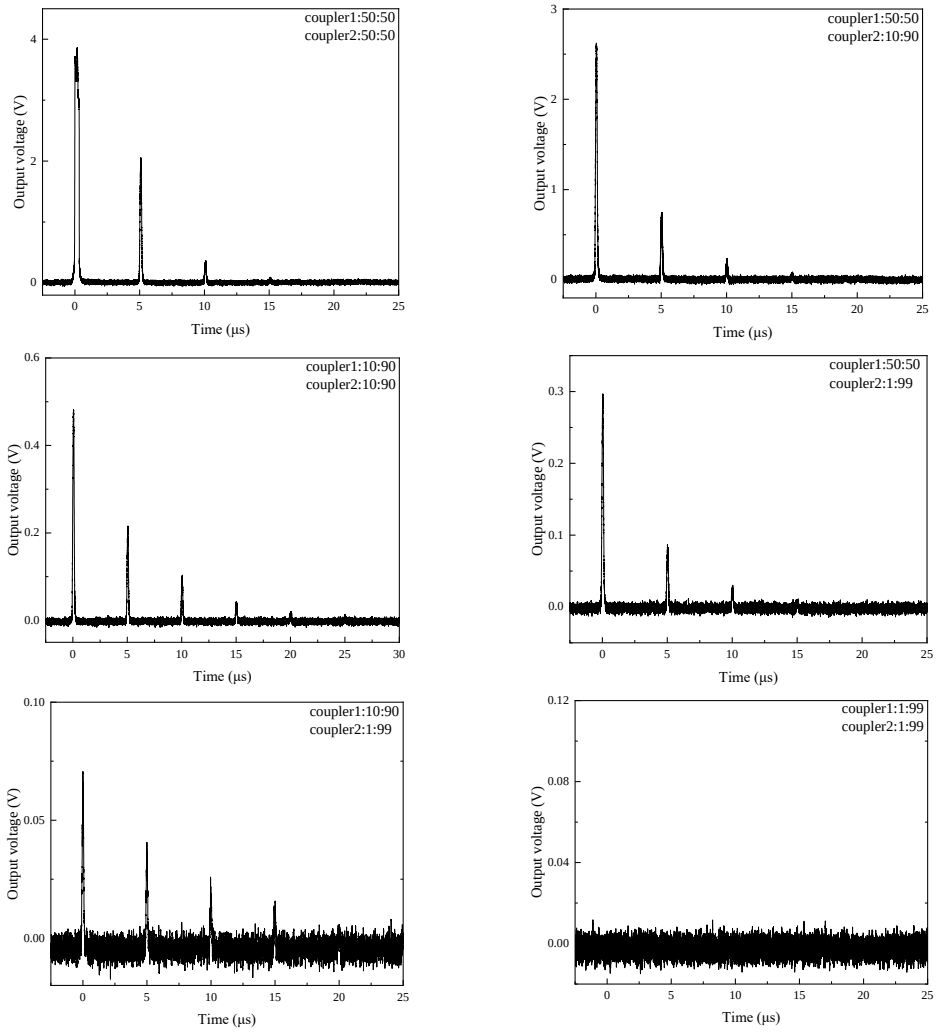

Figure 3. The attenuated pulse waveforms under different collocations of the couplers.

Table 1. The detected signal results under different collocations of the couplers.

No.	Split Ratios of the Couplers	U_1(mV)	U_2(mV)	U_3(mV)	U_4(mV)	U_5(mV)
1	K1 = 0.9, K2 = 0.5	238.700	96.860	33.756	12.693	4.772
2	K1 = 0.5, K2 = 0.5	1193.740	249.371	52.093	10.882	2.273
3	K1 = 0.9, K2 = 0.9	47.749	32.318	21.874	14.805	10.02
4	K1 = 0.5, K2 = 0.99	23.874	9.875	4.084	1.689	0.698
5	K1 = 0.9, K2 = 0.99	4.774	3.555	2.656	1.970	1.467
6	K1 = 0.99, K2 = 0.99	0.477	0.391	0.320	0.262	0.214

It can be seen from Figure 3 that when the split ratio of the two couplers was 10:90, the obtained waveform had the largest number of pulses, which indicated that the laser circulated the most times in the ring cavity and the signal noise was relatively small. Table 1 shows the peak values of the first five pulses of the attenuated pulse waveform obtained in the experiment. The data of No. 3 in the table corresponds to the split ratio of the couplers being 10:90. It can also be seen that although the peak value of the first pulse signal was small, the amplitude of the fifth pulse signal was the largest, compared with the other collocations of the couplers, indicating that the use of this collocation of the couplers had the smallest signal attenuation in the ring cavity. Therefore, two 10:90 couplers were used to conduct the experimental research. On the one hand, the number of interactions between the laser and the gas sensor was greater, which could improve the detection sensitivity, and, on the other hand, the number of pulses was greater, so a more accurate fitting curve could be obtained.

3.2. Detectable SF_6 Decomposition Component Analysis

The detection experiments of several typical SF_6 decomposition components of CO, SO_2, SO_2F_2 and SOF_2 were carried out, and the detection ability of the carbon nanotube-coated fiber gas sensor for the gas components was tested at room temperature, so as to determine the detectable decomposition components. The gas concentrations of 0 ppm, 50 ppm, 100 ppm, 150 ppm, and 200 ppm were selected in the experiment, and the background gas was N_2. According to the influence law of different concentrations of gas on the ring-down time, it was judged whether the gas could be quantitatively detected, and the detectable gas was screened out.

The experimental results are shown in Figure 4. Compared with the other gases, the linear law between CO and ring-down time was stronger. The change of the concentration of SO_2F_2 and SOF_2 basically did not cause the change in the ring-down time. For SO_2, there was a linear law between the concentration and the ring-down time, but the change of the ring-down time was not as obvious as that of CO detection.

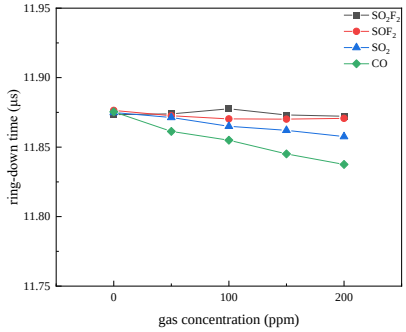

Figure 4. The relationship between gas concentration and ring-down time.

Due to the evanescent field around the micro fiber, it was sensitive to change in the refractive index. When the coating material absorbed gas, its optical properties would also change accordingly, and the refractive index of the cladding would change, resulting in a

decrease in the intensity of light waves transmitted in the micro fiber and an increase in the optical loss of the sensor. The change of optical loss was measured by the FLRD system.

In the process of CO detection, although there may be some SO_2 interference, the selectivity of the sensor could be improved through material modification, and the decoupling algorithm of electrochemical sensors could be used for reference in the future to eliminate the interference effect. In this paper, the detection performance of carbon nanotube-coated fiber gas sensor was explored with CO detection, thus, illustrating the possibility of application of this fiber gas detection method in the power industry.

In the FLRD system, the reason for the decrease of the ring-down time was the increase of the optical loss of the system, indicating that the interaction of CO and carbon nanotubes could lead to increase of the optical loss of the fiber gas sensor. In Figure 4, the change between CO concentration the ring-down time showed a linear law, which could be used to realize the quantitative detection of CO.

3.3. Gas Adsorption Properties

From the above experimental results, combined with the existing research [18], when the nanomaterial adsorbed gas, its dielectric constant would change, which would lead to change in the refractive index of the material and change in the optical loss of the sensor. That is to say, the gas detection capability of the coated fiber gas sensor was related to the adsorption characteristics between nanomaterials and gases. Therefore, based on the density functional theory, the theoretical analysis of the adsorption characteristics between carbon nanotubes and four kinds of gases was carried out, and the above experimental phenomena explained.

The adsorption structures of CO, SO_2, SO_2F_2 and SOF_2 gases and single-walled carbon nanotubes were constructed, and the first-principles optimization carried out, as shown in Figure 5. The $DMol^3$ module of Material Studio was used for calculation, and the adsorption behavior of four kinds of gases on single-walled carbon nanotubes simulated. To calculate the optimization energy and related properties of the architecture of the gas–solid interface, the GGA–PBE functional method was utilized. Dual numerical polarization (DNP) was chosen as the basis set function for linear combination of atomic orbitals (LCAO), and the effect of Van der Waals forces corrected by considering the TS method in DFT–D dispersion correction. Under the condition that the adsorption distance between each gas molecule and single-walled carbon nanotubes was kept the same, the corresponding adsorption energy was calculated. The detailed data are shown in Table 2. According to the adsorption parameters in Table 2, it was judged that single-walled carbon nanotubes had the best adsorption effect on CO molecules under the same conditions, the adsorption energy reaching −0.150 Ha, and the corresponding adsorption distances were both 1.813 Å. In addition, the adsorption energy of SO_2 on single-walled carbon nanotubes was −0.117 Ha. Among the four gases, its adsorption capacity was only weaker than that of CO, which also explained why the carbon nanotube-coated fiber responded to SO_2 in the above experiment. The adsorptions of SO_2F_2 and SOF_2 were weak, so maybe only high concentrations of SO_2F_2 and SOF_2 could be detected. The simulation calculation results explained the reason why the carbon nanotube-coated fiber gas sensor could detect CO. Next, the detection performance of CO gas was analyzed.

Table 2. Adsorption energies of four gas molecules on single-walled carbon nanotubes.

Structures	$E_{molecule}$/Ha	E_{SWNT}/Ha	$E_{molecule+SWNT}$/Ha	Ead/Ha
CO	−113.232	−2437.119	−2550.201	−0.150
SO_2	−548.413	−2437.119	−2985.415	−0.117
SO_2F_2	−748.005	−2437.119	−3185.009	−0.115
SOF_2	−672.831	−2437.119	−3109.840	−0.110

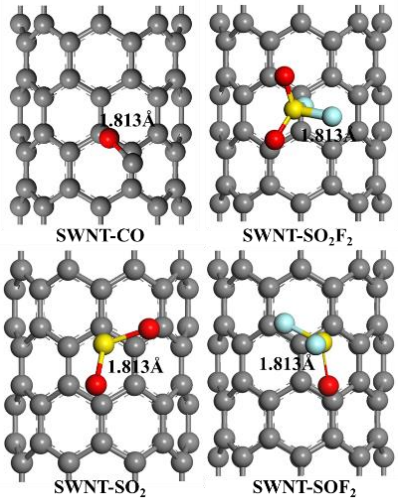

Figure 5. Adsorption structures of four gas molecules on single-walled carbon nanotubes.

3.4. CO Detection Performance Analysis

3.4.1. Linear Fitting and Concentration Inversion

During the experiment, the background gas, N_2, was first introduced into the gas detection cell. After the airflow was stable, the pulse waveform was recorded with an oscilloscope, as shown in Figure 6. Then, CO gas, with concentrations of 50 ppm, 100 ppm, 150 ppm and 200 ppm, were introduced into the gas detection cell, and the original waveform recorded. When the gas concentration changed, the pulse signal also changed. Taking the peak value of the pulse signal and the corresponding time, exponential function fitting was performed, and the ring-down curve under different concentrations was obtained, as shown in Figure 7. It can be seen that as the concentration increased, the ring-down curve also changed regularly.

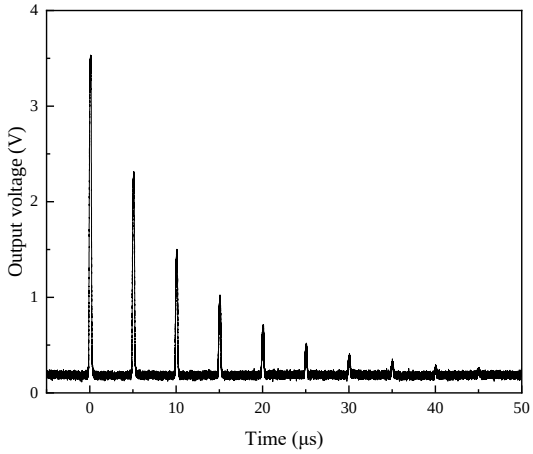

Figure 6. Original waveform under N_2 background gas.

According to the fitting results of the exponential function, the ring-down time corresponding to different concentrations of CO was obtained, and the linear fitting between the concentration and the ring-down time was performed by the least squares method, as shown in Figure 8. It can be seen that there was a good linear relationship between the ring-down time and the gas concentration, with R^2 being 0.984.

Then, after establishing the relationship between gas concentration and ring-down time, to form the quantitative method, the CO gas, with concentrations of 25 ppm, 75 ppm, 125 ppm and 175 ppm, was introduced into the gas detection cell, and the inversion calculation performed. The error analysis of the quantitative method was carried out, and the results are shown in Table 3. It can be seen that the maximum error between the

inversion result and the real value was 1.916 ppm, and the maximum relative error was 4.10%, which exhibited good measurement accuracy.

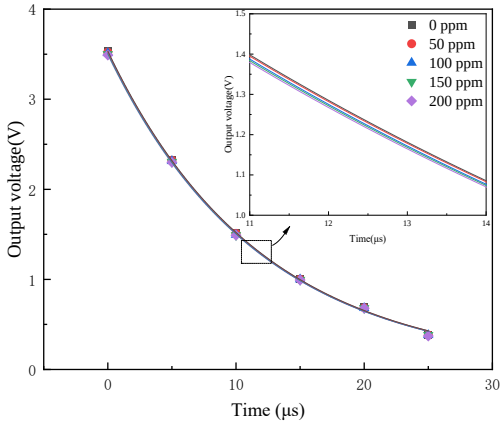

Figure 7. Fitting curve of exponential function corresponding to different CO concentrations.

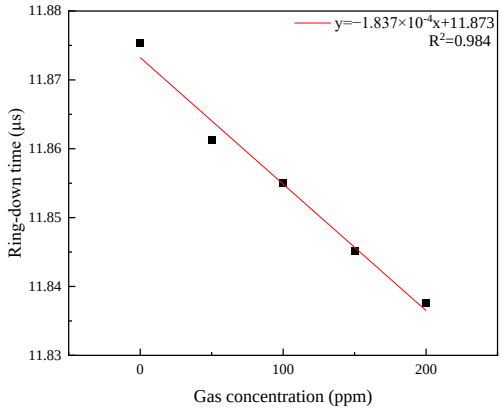

Figure 8. The relationship between the ring-down time and the gas concentration.

Table 3. The concentration inversion and error analysis.

Actual Concentration (ppm)	Inversion Concentration (ppm)	Relative Error (%)
25	23.975	4.10
75	75.504	0.67
125	123.084	1.53
175	175.257	0.15

3.4.2. Sensitivity Analysis

Sensitivity reflects the change of the output relative to the input. For the FLRD system in this paper, the change of ring-down time was used to reflect the change of gas concentration. Therefore, the sensitivity of the FLRD system could be defined as the change degree of the ring-down time τ caused by the change of the gas concentration C to be measured, which could be expressed by the following equation:

$$S = \Delta\tau/\Delta C \quad (1)$$

In the equation, S represents the sensitivity, $\Delta\tau$ represents the variation of the ring-down time, and ΔC represents the variation of the concentration. From Equation (1), the sensitivity of the system was 0.183 ns/ppm.

3.4.3. Detection Limit Analysis

There are few related studies on the detection limit of the FLRD gas detection system. In this paper, a method for solving the gas detection limit is proposed. The detection limit represents the lowest gas concentration that the system can measure. From the above CO detection results, it could be found that, in the FLRD system, increase of CO concentration led to an increase in the optical loss of the fiber gas sensor, resulting in an increase in the overall loss of the system, a decrease in the amplitude of the optical pulse signal in the original waveform, and a decrease in the ring-down time. According to the FLRD system principle, the equation for the ring-down time is as follows:

$$I = I_0 e^{-\frac{t}{\tau}} \tag{2}$$

$$\tau = \frac{nL}{c(A+B)} \tag{3}$$

In the equation, I represents the light intensity of the output light received by the PD, which decays exponentially with time, I_0 represents the initial light intensity, t represents the time, τ represents the ring-down time, c represents the speed of light in vacuum, n represents the refractive index of the single-mode fiber, L represents the length of the fiber ring cavity, A represents the inherent loss of the system, and B represents the optical loss generated by the fiber gas sensor.

In the actual measurement, the light intensity was converted into the electrical signal by the PD, and then acquired by the oscilloscope, so Equation (2) could be expressed as:

$$U = U_0 e^{-\frac{t}{\tau}} \tag{4}$$

In the equation, U and U_0 represent the electrical signals obtained by the PD. respectively, for the light intensity of the output light and the initial light intensity. During the experiment, the original waveform was generally composed of multiple pulse signals, as shown in Figure 6. Taking the pulse signal amplitudes at different times t, and fitting Equation (4) to obtain the ring-down curves at different concentrations, the ring-down time τ could be obtained, and, then, the concentration inversion calculation performed.

When the gas concentration was very low, the increase in the optical loss B of the fiber gas sensor was small, which made the change in the ring-down time τ small. At this time, the amplitude of the optical pulse signal in the original waveform would be closer to the amplitude of the optical pulse signal under the background gas. When the change in amplitude of the optical pulse signal, caused by a certain gas concentration value, could just be resolved, the value of the ring-down time τ with the smallest change could be calculated accordingly, and the concentration obtained by inversion was the detection limit of the system.

The number of optical pulses in the original pulse signal was generally 5 to 9, and the pulse signal with the most obvious pulse amplitude change with concentration change selected as the optical pulse signal for judging the detection limit. In the ring-down curves of different sensor optical losses, the voltage signal changed most obviously in the middle time period. Figure 9 shows the simulation results of the ring-down curve of the FLRD system under the different sensor optical losses. Assuming that the optical losses corresponding to the different ring-down curves were $a_5 > a_4 > a_3 > a_2 > a_1$, it could be seen that when the time was between 5~20 μs, with the increase of the loss, and the voltage value changed more obviously.

In order to accurately obtain the time corresponding to the maximum voltage change under the different sensor losses, it was necessary to solve the voltage difference between the ring-down curve under the background gas and the ring-down curve under different

sensor optical losses, and find the time corresponding to the maximum voltage difference. Equation (5) could be used to solve this:

$$\Delta U = U_b - U_n = U_0 e^{-\frac{t}{\tau_b}} - U_0 e^{-\frac{t}{\tau_n}} \quad (5)$$

In the equation, ΔU represents the voltage difference, and U_b and τ_b represent the voltage value and the ring-down time of the ring-down curve under the background gas. The values U_n and τ_n represent the voltage value and the ring-down time of the ring-down curve under the different optical losses of the sensor. Let n be 1, 2, 3, 4, 5, $\tau_1 > \tau_2 > \tau_3 > \tau_4 > \tau_5$. Then, the curve of the voltage difference between the background gas ring-down curve and the ring-down curve under the different optical losses could be obtained, as shown in Figure 10. It can be seen that when the time t was 11.7 μs, the voltage difference had the largest variation. Therefore, the pulse signal closest to the time value was the pulse signal with the largest voltage signal change, due to the change of optical loss, which could be used as the pulse signal for judging the detection limit.

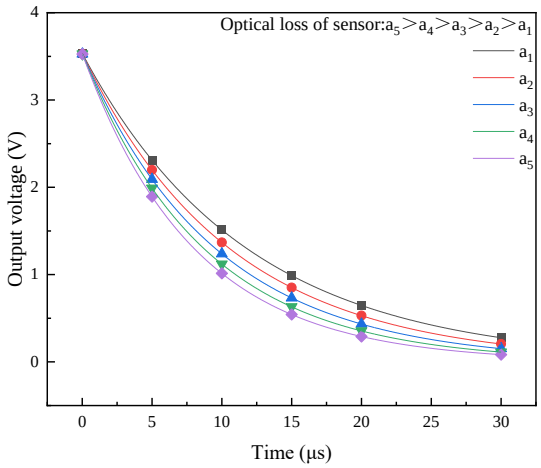

Figure 9. Ring-down curves under the different sensor optical losses.

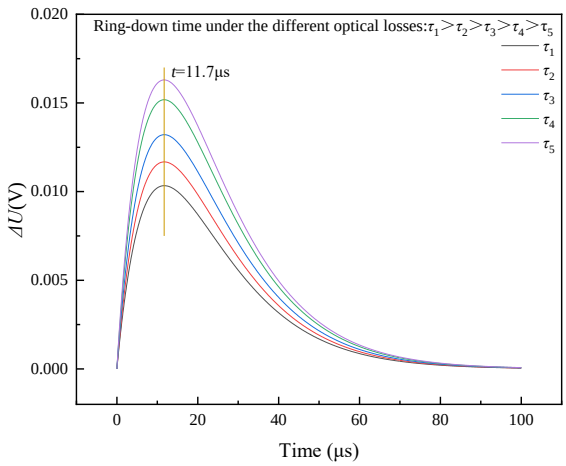

Figure 10. The curve of the voltage difference between the background gas ring-down curve and the ring-down curve under the different optical losses.

Through analysis of the experimental results, it was found that the amplitude of the third pulse signal in the original signal had the largest change with the concentration change. Therefore, it could be defined that the detection limit of the system was that the third pulse signal amplitude difference between the background gas and the detection limit

concentration value was not less than the instrument resolution, which could be expressed by the following equation:

$$\Delta U_{p3} = U_0 e^{-\frac{t_{p3}}{\tau_b}} - U_0 e^{-\frac{t_{p3}}{\tau_{min}}} \geq V_{min} \quad (6)$$

In the equation, ΔU_{p3} represents the amplitude difference of the third pulse signal. V_{min} represents the instrument resolution. The oscilloscope was a Tektronix MSO44, and the resolution was 1 mV. The value t_{p3} represents the time corresponding to the third pulse signal and τ_{min} represents the ring-down time corresponding to the detection limit concentration value. By substituting τ_{min} into the fitting curve of the ring-down time and CO concentration, the detection limit of the system for CO could be calculated. After calculation, the detection limit of CO for the system was 19.951 ppm.

3.4.4. Stability Analysis

The repeatability of single-point measurement refers to the degree of difference between repeated measurements of the same measure and under the same working conditions, expressed as the relative standard deviation of multiple measurements. CO gas with a concentration of 100 ppm was introduced into the gas detection cell, and the value recorded after the gas concentration in the gas detection cell stabilized. The ring-down time was calculated and the result is shown in Figure 11. The standard deviation of single-point repeatability was 0.00356, indicating that the detection system had good single-point repeatability.

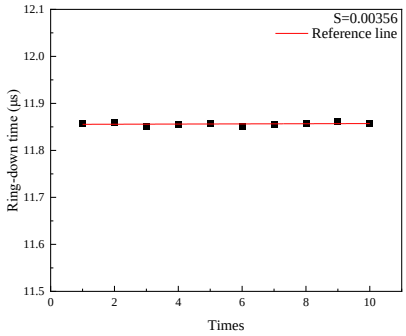

Figure 11. The repeatability of single-point measurement.

Stability refers to the ability of the detection system to remain constant for a specified period when its performance remains constant under specified working conditions. In the stability experiment, CO gas with a concentration of 100 ppm was introduced into the gas detection cell. After it stabilized, the value was recorded every 5 min and its ring-down time calculated. The results are shown in Figure 12. It can be seen that after a long period of experiment, the ring-down time fluctuated slightly, and the standard deviation was 0.00606. Therefore, the detection system had good stability.

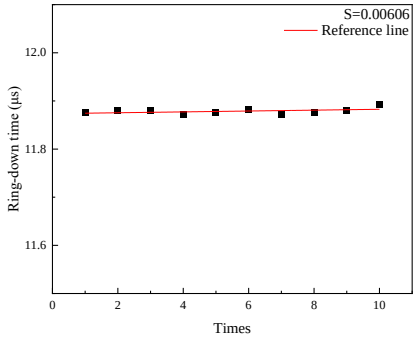

Figure 12. Stability test.

4. Conclusions

In this paper, a carbon nanotube-coated fiber gas sensor was proposed, which has the potential to act as a built-in sensor for online monitoring of SF_6 decomposition components in SF_6 electrical equipment. A CO gas detection method, based on a coated fiber gas sensor, was realized in the FLRD system, which could also provide technical reference for other fields with CO detection needs. The following conclusions were obtained:

1. Among the four typical SF_6 decomposition components of SO_2, SO_2F_2 and SOF_2 and CO, the carbon nanotube-coated fiber gas sensor is more sensitive to CO gas. From the theoretical analysis of the adsorption properties of the material, single-walled carbon nanotubes have the best adsorption effect on CO molecules under the same conditions.

2. The FLRD system, based on the carbon nanotube-coated fiber gas sensor, can realize CO detection at room temperature. With increase of CO concentration, its optical loss gradually increases. There is a good linear relationship between the 0~200 ppm CO and the ring-down time, with R^2 being 0.984.

3. The carbon nanotube-coated fiber gas sensor combined with the FLRD detection system can achieve quantitative detection of 0~200 ppm CO, with a maximum error of 1.916 ppm and a maximum relative error of 4.10%. The sensitivity of the system is 0.183 ns/ppm, and the detection limit of the system is 19.951 ppm. It has good detection stability, the standard deviation of single-point repeatability is 0.00356, and the standard deviation of long period of experiment is 0.00606.

In the future, various gas-sensitive nanomaterials could be used to study the detection ability of nanomaterial-coated fiber gas sensors for SF_6 decomposition components. At the same time, in-depth research on gas detection performance optimization methods could be conducted from the aspects of micro-fiber structural parameters and demodulation technology. The feasibility of multi-SF_6 decomposition component detection in multi-fiber gas sensor distributed sensing could be explored.

Author Contributions: Conceptualization, Y.Z. and X.Z.; methodology, W.Y.; validation, D.W. and R.Z.; writing—original draft preparation, Y.Z.; writing—review and editing, Y.Z. and M.F. All authors have read and agreed to the published version of the manuscript.

Funding: The current work was supported by the Natural Science Foundation of Hubei Province (no. 2022CFB863). The author also gives thanks for the support from the United Laboratory of Advanced Electrical Materials and Equipment Support Technology, CSG.

Institutional Review Board Statement: Not applicable.

Informed Consent Statement: Not applicable.

Data Availability Statement: Not applicable.

Conflicts of Interest: The authors declare no conflict of interest.

References

1. Wu, Y.; Ding, D.; Wang, Y.; Zhou, C.; Lu, H.; Zhang, X. Defect Recognition and Condition Assessment of Epoxy Insulators in Gas Insulated Switchgear Based on Multi-information Fusion. *Measurement* **2022**, *190*, 110701. [CrossRef]
2. Zhang, X.; Zhang, Y.; Tang, J.; Cui, Z.; Li, Y.; Zhou, H.; Zhang, G.; Yang, J. Optical technology for detecting the decomposition products of SF6: A review. *Opt. Eng.* **2018**, *57*, 110901. [CrossRef]
3. Zeng, F.; Li, H.; Cheng, H.; Tang, J.; Liu, Y. SF_6 decomposition and insulation condition monitoring of GIE: A review. *High Volt.* **2021**, *6*, 955–966. [CrossRef]
4. Tang, J.; Yang, X.; Yao, Q.; Miao, Y.; She, X.; Zeng, F. Correlation analysis between SF6 decomposed components and negative DC partial discharge strength initiated by needle-plate defect. *IEEJ Trans. Electr. Electron. Eng.* **2018**, *13*, 382–389. [CrossRef]
5. Mahdi, A.S.; Abdul-Malek, Z.; Arshad, R.N. SF_6 Decomposed Component Analysis for Partial Discharge Diagnosis in GIS: A Review. *IEEE Access* **2022**. [CrossRef]
6. Yang, R.; Xu, M.; Guan, C.; Yan, J.; Geng, Y.C. Influence of trace H_2O and O_2 on SF_6 decomposition products under arcing conditions in electric power equipment. *J. Eng.* **2019**, *2019*, 1774–1777. [CrossRef]
7. Fan, X.; Li, L.; Zhou, Y.; Tang, N.; Zou, Z.; Li, X.; Huang, G.; Liu, M. Online detection technology for SF_6 decomposition products in electrical equipment: A review. *IET Sci. Meas. Technol.* **2018**, *12*, 707–711. [CrossRef]

8. Zhuang, Y.; Hu, X.; Tang, B.; Wang, S.; Cui, A.; Hou, K.; He, Y.; Zhu, L.; Li, W.; Chu, J. Effects of SF_6 decomposition components and concentrations on the discharge faults and insulation defects in GIS equipment. *Sci. Rep.* **2020**, *10*, 1–12. [CrossRef]
9. Zhang, X.; Zhang, J.; Jia, Y.; Xiao, P.; Tang, J. TiO_2 nanotube array sensor for detecting the SF_6 decomposition product SO_2. *Sensors* **2012**, *12*, 3302–3313. [CrossRef]
10. Gui, Y.; Zhang, X.; Lv, P.; Wang, S.; Tang, C.; Zhou, Q. Ni-CNT chemical sensor for SF_6 decomposition components detection: A combined experimental and theoretical study. *Sensors* **2018**, *18*, 3493. [CrossRef]
11. Li, L.; Din, S.U.; ul Haq, M.; Tang, N.; Zhang, M.; Rahman, N.; Zhu, L. Room temperature monitoring of SF_6 decomposition byproduct SO_2F_2 based on $TiO_2/NiSO_4$ composite nanofibers. *Nanotechnology* **2021**, *32*, 305705. [CrossRef]
12. Zhang, X.; Yan, J.; Zhang, Y.; Cheng, L.; Bian, C.; Chen, X. Infrared Spectrum Analysis and Quantitative Detection of SF_6 Characteristic Decomposition Components SO_2F_2 and SOF_2. *IEEE Trans. Dielectr. Electr. Insul.* **2022**, *29*, 1316–1323. [CrossRef]
13. Chen, Z.; Zhang, X.; Yang, T.; Fan, S.; Cheng, H.; Xu, G.; Zhang, Y.; Zhou, H. Detection of trace carbon monoxide based on cantilever enhanced photoacoustic spectroscopy at 2.33 μm. *Infrared Phys. Technol.* **2022**, *126*, 104364. [CrossRef]
14. Zhang, X.; Liu, H.; Ren, J.; Li, J.; Li, X. Fourier transform infrared spectroscopy quantitative analysis of SF_6 partial discharge decomposition components. *Spectrochim. Acta Part A Mol. Biomol. Spectrosc.* **2015**, *136*, 884–889. [CrossRef] [PubMed]
15. Joe, H.-E.; Yun, H.; Jo, S.-H.; Jun, M.B.G.; Min, B.-K. A review on optical fiber sensors for environmental monitoring. *Int. J. Precis. Eng. Manuf. Green Technol.* **2018**, *5*, 173–191. [CrossRef]
16. Gao, X.; Ning, T.; Zhang, C.; Xu, J.; Zheng, J.; Lin, H.; Li, J.; Pei, L.; You, H. A dual-parameter fiber sensor based on few-mode fiber and fiber Bragg grating for strain and temperature sensing. *Opt. Commun.* **2020**, *454*, 124441. [CrossRef]
17. Jia, L.; Wu, Y.; Yao, B.; Yang, F.; Rao, Y. A sensitivity enhanced gas sensor based on carbon nanotubes around microfiber. In Proceedings of the Third Asia Pacific Optical Sensors Conference, SPIE, Sydney, NSW, Australia, 31 January–3 February 2012; Volume 8351, pp. 457–463.
18. Yao, B.; Wu, Y.; Jia, L.; Rao, Y.; Gong, Y.; Jiang, C. Mode field distribution of optical transmission along microfiber affected by CNT films with complex refraction index. *JOSA B* **2012**, *29*, 891–895. [CrossRef]
19. Ashkavand, Z.; Sadeghi, E.; Parvizi, R.; Zare, M. Developed low-temperature anionic 2H-MoS_2/Au sensing layer coated optical fiber gas sensor. *ACS Appl. Mater. Interfaces* **2020**, *12*, 34283–34296. [CrossRef]
20. Zhou, Z.; Xu, Y.; Qiao, C.; Liu, L.; Jia, Y. A novel low-cost gas sensor for CO_2 detection using polymer-coated fiber Bragg grating. *Sens. Actuators B Chem.* **2021**, *332*, 129482. [CrossRef]
21. Yu, C.; Wu, Y.; Liu, X.; Fu, F.; Gong, Y.; Rao, Y.-j.; Chen, Y. Miniature fiber-optic NH_3 gas sensor based on Pt nanoparticle-incorporated graphene oxide. *Sens. Actuators B Chem.* **2017**, *244*, 107–113. [CrossRef]
22. Fu, H.; Wang, Q.; Ding, J.; Zhu, Y.; Zhang, M.; Yang, C.; Wang, S. Fe_2O_3 nanotube coating micro-fiber interferometer for ammonia detection. *Sens. Actuators B Chem.* **2020**, *303*, 127186. [CrossRef]